

# Atomic Force Microscopy Probing of Receptor–Nanoparticle Interactions for Riboflavin Receptor Targeted Gold–Dendrimer Nanocomposites

Amanda B. Witte,<sup>†,||</sup> Abigail N. Leistra,<sup>†,||</sup> Pamela T. Wong,<sup>‡,§</sup> Sophia Bharathi,<sup>‡,§</sup> Kevin Refior,<sup>‡</sup> Phillip Smith,<sup>‡</sup> Ola Kaso,<sup>‡</sup> Kumar Sinniah,<sup>\*,†</sup> and Seok Ki Choi<sup>\*,‡,§</sup>

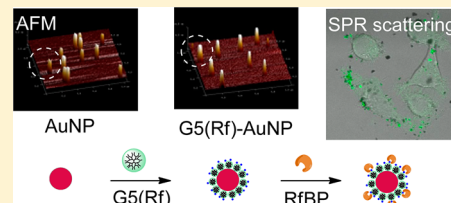
<sup>†</sup>Department of Chemistry & Biochemistry, Calvin College, 3201 Burton Street SE, Grand Rapids, Michigan 49546, United States

<sup>‡</sup>Michigan Nanotechnology Institute for Medicine and Biological Sciences, University of Michigan, Ann Arbor, Michigan 48109, United States

<sup>\*</sup>Department of Internal Medicine, University of Michigan, Ann Arbor, Michigan 48109, United States

## Supporting Information

**ABSTRACT:** Riboflavin receptors are overexpressed in malignant cells from certain human breast and prostate cancers, and they constitute a group of potential surface markers important for cancer targeted delivery of therapeutic agents and imaging molecules. Here we report on the fabrication and atomic force microscopy (AFM) characterization of a core–shell nanocomposite consisting of a gold nanoparticle (AuNP) coated with riboflavin receptor-targeting poly(amido amine) dendrimer. We designed this nanocomposite for potential applications such as a cancer targeted imaging material based on its surface plasmon resonance properties conferred by AuNP. We employed AFM as a technique for probing the binding interaction between the nanocomposite and riboflavin binding protein (RFBP) in solution. AFM enabled precise measurement of the AuNP height distribution before (13.5 nm) and after chemisorption of riboflavin-conjugated dendrimer (AuNP–dendrimer; 20.5 nm). Binding of RFBP to the AuNP–dendrimer caused a height increase to 26.7 nm, which decreased to 22.8 nm when coincubated with riboflavin as a competitive ligand, supporting interaction of AuNP–dendrimer and its target protein. In summary, physical determination of size distribution by AFM imaging can serve as a quantitative approach to monitor and characterize the nanoscale interaction between a dendrimer-covered AuNP and target protein molecules *in vitro*.



## INTRODUCTION

Gold nanoparticles (AuNPs)<sup>1,2</sup> belong to a class of nanometer-sized gold structures that display unique photothermal and optical properties due to their surface plasmon resonance (SPR).<sup>3–9</sup> Surface fabrication of AuNPs as a core–shell hybrid nanostructure allows applications of such properties in the design of catalysts,<sup>2</sup> sensors,<sup>10–12</sup> imaging devices,<sup>3–5,13</sup> photothermal agents,<sup>6–9</sup> and delivery systems of genes<sup>14</sup> and therapeutic agents<sup>8,15</sup> for targeted therapy. A large fraction of these studies have focused on exploring new functional applications of the AuNP-based nanoparticles based on their photophysical properties. However, three-dimensional features that vary in response to the interaction between AuNP-based nanoparticles and their biological targets such as particle size distribution can provide physical insights on their interaction although they remain much less characterized in most AuNP-based delivery systems.<sup>16,17</sup> Here, we studied the interaction of a dendrimer chemisorbed AuNP with its protein target by atomic force microscopy (AFM) as a biophysical method to correlate protein binding with the geometrical alteration of the AuNP nanocomposite. This study demonstrates that AFM serves as an effective technique for characterizing the interaction of AuNP-based nanoparticles and target proteins *in vitro* by quantitative measurement of size distribution.

Dendrimer NPs used for surface modification of AuNPs are based on a fifth generation (G5) poly(amido amine) (PAMAM) dendrimer conjugated with a riboflavin (RF) molecule. As a vitamin molecule ( $B_2$ ) essential for the biosynthesis of flavin-based redox cofactors, RF is taken up by riboflavin receptors, also referred to as RF carriers, which are expressed as both soluble and membrane-bound isoforms.<sup>18</sup> Moreover, RF receptors constitute one type of potential tumor biomarker due to their overexpression in certain malignant cells from human breast and prostate cancers.<sup>19,20</sup> This biomarker is relatively new as a receptor considered for cancer targeting compared to other biomarker proteins that include folic acid receptor (FAR),<sup>21–23</sup>  $\alpha_{v}\beta_3$  integrin,<sup>24–26</sup> prostate-specific membrane antigen,<sup>27</sup> HER2 receptor,<sup>28</sup> and epidermal growth factor receptor.<sup>28–30</sup> Recently, we applied the concept of targeted drug delivery to the RF receptor by designing RF-conjugated PAMAM dendrimer nanoparticles and demonstrated their effectiveness *in vitro* for RF receptor targeted delivery of methotrexate (MTX) in KB cancer cells that overexpress the riboflavin receptors.<sup>31–33</sup>

Received: December 9, 2013

Revised: February 23, 2014

Published: February 26, 2014

In a follow-up study,<sup>32</sup> we employed isothermal titration calorimetry (ITC) and differential scanning calorimetry (DSC) to address the thermodynamic aspects of the RF receptor-ligand interactions for RF-conjugated dendrimers. Combination of these two methods provided biophysical information important for the correlation of binding affinity to design factors such as ligand valency and the RF attachment position of the dendrimer conjugates. These studies allowed characterization of the structural features dictating the thermodynamic aspects of the interaction between the dendrimer and the receptor protein.

In the current study, we employed AFM for structural characterization of RF receptor targeted AuNP systems. AFM has been used for the imaging of PAMAM dendrimer NPs<sup>34–36</sup> of various dendrimer sizes. The rigidity of generation 7 or higher dendrimers makes it possible to image them by AFM,<sup>35</sup> whereas the softer G5 dendrimers used for RF conjugation ( $d = 5.4 \text{ nm}$ )<sup>37</sup> in this study tend to flatten on mica surfaces, providing fuzzy AFM images. Thus we designed a larger AuNP–dendrimer hybrid nanoparticle for this AFM study. First, AuNP brings a number of photophysical and photo-thermal properties, and its surface functionalization with the dendrimer platform creates a hybrid nanosystem that enables both imaging and specific cancer targeting. Second, in contrast to the soft dendrimer, the AuNP provides advantages for performing the AFM study primarily because it can serve as a marker, due to its metallic core and can be obtained in sizes greater than the dendrimer NP. Hence AFM is ideally suited for the determination of the size alteration as a quantifiable physical property that follows binding of the target protein to the dendrimer-conjugated AuNP. Recently, structural characterization of AuNP hybrids by AFM has been demonstrated for a number of AuNP hybrid systems, each AuNP conjugated with oligonucleotide (DNA) probes,<sup>38,39</sup> polyphenylene dendrimer,<sup>40</sup> PEG,<sup>41</sup> poly(4-vinylpyridine),<sup>42</sup> and cyclodextrin.<sup>43</sup> Finally, AFM can image surfaces with nanoscale resolution, and unlike other imaging techniques such as transmission electron microscopy (TEM), it can image a variety of biomacromolecular complexes and biological events under nearly physiological conditions.<sup>44,45</sup> As a result, AFM has been widely applied to numerous applications in biology and drug discovery.<sup>46–49</sup>

The present report focuses on AFM characterization of AuNPs functionalized on the surface with dendrimer NPs as a new class of RF receptor targeted delivery systems. This AFM study was performed in combination with complementary techniques including UV-vis spectrometry and in vitro confocal microscopy to image binding of the dendrimer-functionalized AuNPs to riboflavin receptor in a cancer cell. This study illustrates how physical measurement of particle size distribution of AuNPs by AFM enables the characterization and precise monitoring of the biological interaction between a dendrimer conjugated AuNP and its target protein in a physiological solution.

## ■ EXPERIMENTAL SECTION

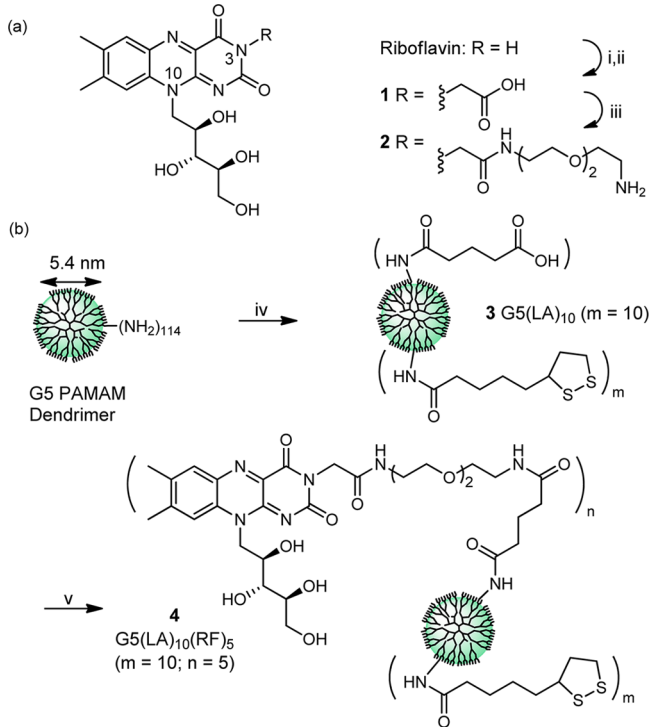
**Materials.** Unless noted otherwise, all reagents and solvents were purchased from Sigma-Aldrich including ( $\pm$ )- $\alpha$ -lipoic acid ( $\geq 98\%$ ), (−)-riboflavin ( $\geq 98\%$ ), riboflavin binding protein (*apo*-form), 3-(aminopropyl)triethoxysilane, and gold(III) chloride trihydrate ( $\geq 99.9\%$ ). A fifth generation (G5) PAMAM dendrimer (G5-NH<sub>2</sub>) was purchased from Dendritech, Inc. (Midland, MI) as a solution in methanol (17.5% by

wt/wt). It was purified by dialysis against deionized water prior to use as described elsewhere.<sup>50,51</sup> The mean number ( $n = 114$ ) of primary amines per G5-(NH<sub>2</sub>)<sub>n</sub> was determined by potentiometric titration<sup>52</sup> using a Mettler Toledo MP230 pH meter equipped with an InLab Micro electrode.

**Methods.** Each modified dendrimer was purified by dialysis using cellulose membrane tubing from Spectrum Laboratories (MWCO 10 000). Each dendrimer, including the parent and surface-modified G5 dendrimers, was fully characterized by a number of standard analytical methods as described below.<sup>32,50,51,53</sup> NMR characterization of the dendrimers was performed at 500 MHz for <sup>1</sup>H nucleus using a Varian NMR spectrometer.<sup>50,53</sup> <sup>1</sup>H NMR spectra are reported in ppm relative to an internal standard 2,2-dimethyl-2-silapentane-5-sulfonate sodium salt (DSS;  $\delta = 0.00 \text{ ppm}$ ). Molecular weights of dendrimers conjugated with lipoic acid and riboflavin were determined by matrix-assisted laser desorption ionization time-of-flight (MALDI TOF) mass spectrometry with a Waters TofsPec-2E spectrometer (MW for a parent G5 dendrimer = 27 600 g/mol).<sup>51</sup> UV-vis spectrometry was performed on a Perkin-Elmer Lambda 20 spectrophotometer. The purity of each dendrimer was determined by ultraperformance liquid chromatography (UPLC) on a Waters Acuity Peptide Mapping System equipped with a Waters photodiode array detector.<sup>51</sup> Each sample was run on a C4 BEH column (150 × 2.1 mm, 300 Å) with a linear gradient method beginning with 98:2 (v/v) water/acetonitrile (with trifluoroacetic acid at 0.14 wt % in each eluent) at a flow rate of 1 mL/min. Molecular weights ( $M_w$ ,  $M_n$ ) and polydispersity index values (PDI =  $M_w/M_n$ ) of G5 PAMAM dendrimer were determined by gel permeation chromatography (GPC), and details for the experimental method are already described earlier.<sup>50,51</sup> The PDI value determined for the purified G5 dendrimer was 1.010 ( $M_n = 26\,270 \text{ g/mol}$ ). The size distribution of gold nanoparticles (AuNPs) was determined by dynamic light scattering measured at 25 °C on a Zetasizer Nano ZS (Malvern).

**Synthesis of the 3 G5(LA)<sub>10</sub> Conjugate (Scheme 1).** To a solution of ( $\pm$ )-lipoic acid (29 mg, 0.14 mmol) in DMF (5 mL) was added *N*-hydroxybenzotriazole (HOEt; 22 mg, 0.14 mmol), *N,N'*-diisopropylethylamine (DIPEA; 49 μL, 0.28 mmol) and *N*-(3-dimethylaminopropyl)-*N'*-ethylcarbodiimide hydrochloride (EDC; 56 mg, 0.29 mmol). The reaction mixture was stirred at room temperature (RT) for 4 h. G5 PAMAM dendrimer (250 mg, 9.4 μmol) was dissolved in MeOH (100 mL) in a separate reaction flask. To this dendrimer solution was then added the activated ester of lipoic acid prepared above while the mixture was stirred. The final mixture was stirred for 15 h, and excess unreacted amine groups of the dendrimer were fully modified by reacting with glutaric anhydride (210 mg, 1.84 mmol) and DIPEA (310 μL, 1.8 mmol). After stirring for 6 h, the mixture was concentrated in vacuo, and the residue was dissolved in 10 mL of phosphate buffered saline (PBS, pH 7.4). The solution was loaded into a membrane dialysis bag (MWCO 10 kDa), and dialyzed against PBS (2 × 2L) and deionized water (3 × 2L) over 2 days until its dendrimer purity was greater than 95% as determined by analytical UPLC. The dialyzed solution was collected and freeze-dried to afford 3 G5(LA)<sub>10</sub> as a pale beige solid (378 mg). UPLC:  $t_r = 8.8 \text{ min}$ ; purity >95%. MALDI TOF determined molecular weight (*m/z*, g mol<sup>−1</sup>): 40 700. <sup>1</sup>H NMR (500 MHz, D<sub>2</sub>O):  $\delta$  3.44–3.36 (broad), 3.32 (br s), 3.06–2.9 (br), 2.86–2.72 (br), 2.56–2.46 (br), 2.28–2.23 (br t), 2.2–2.17 (br t), 1.86–1.79 (br quin),

**Scheme 1.** (a) Synthesis of Riboflavin (RF) Derivative 2 Terminated with a Primary Amine at the Linker Installed at the N3 Position of RF and (b) Preparation of Generation 5 (G5) Poly(amido amine) (PAMAM) Dendrimers 3 and 4 G5(LA)<sub>10</sub>(RF)<sub>5</sub> Each Presenting 10 Molecules of Lipoic Acid (LA), in Combination with an Average of 5 Molecular Copies of Riboflavin (RF)<sup>a,b</sup>,



<sup>a</sup>The theoretical number of terminal branches per G5 dendrimer is 128 (experimentally, 114 based on potentiometric titration<sup>50</sup>), but only a fraction of the branches are shown for clarity. In conjugates 3 and 4, each branch is terminated with a glutaric acid group unless its carboxylic acid is further conjugated with LA or RF. <sup>b</sup>Reagents and conditions: (i) ethyl bromoacetate, K<sub>2</sub>CO<sub>3</sub>, DMF, 85 °C; (ii) 6 M HCl, 90 °C; (iii) 2,2'-(ethylenedioxy)bis(ethylamine), PyBOP, HOBr, N,N'-diisopropylethylamine, DMF, rt; (iv) (a) EDC-HCl, HOBr, N,N'-diisopropylethylamine, (±)-lipoic acid, rt; (b) glutaric anhydride (180 equiv to dendrimer), N,N'-diisopropylethylamine (180 equiv); (v) (a) PyBOP, HOBr, N,N'-diisopropylethylamine, DMF, rt; (b) 2 (8 equiv), 24 h, rt.

1.6 (br m), 1.4 (br m) ppm (abbreviation: br = broad; s = singlet; t = triplet; quin = quintet; m = multiplet).

**Synthesis of the 4 G5(LA)<sub>10</sub>(RF)<sub>5</sub> Conjugate (Scheme 1).** N3-Carboxymethylriboflavin **1**<sup>31,54,55</sup> was first converted to its linker-extended form **2** prior to its conjugation with **3** G5(LA)<sub>10</sub>. To a stirred solution of N3-carboxymethylriboflavin (15 mg, 35 μmol) dissolved in DMF (9 mL) was added HOBr (6.4 mg, 42 μmol), DIPEA (12 μL, 69 μmol) and PyBOP (22 mg, 42 μmol) sequentially. The reaction mixture was stirred at RT for 17 h, followed by addition of 2,2'-(ethylenedioxy)bis(ethylamine) (5.1 μL, 34 μmol). After stirring for an additional 7 h, product **2** in the reaction mixture was used for dendrimer conjugation in the next step without further treatment as described below. To a mixture of G5(LA)<sub>10</sub> (50 mg, 1.2 μmol), HOBr (33 mg, 216 μmol), and DIPEA (50 μL, 287 μmol) in DMF (5 mL) was added PyBOP (111 mg, 213 μmol). The mixture was stirred for 20 h at RT prior to the addition of **2** in DMF (2.4 mL; prepared above). After stirring for an additional

24 h, the reaction mixture was concentrated in vacuo, and the residue was dissolved in 10 mL of phosphate buffered saline (PBS, pH 7.4). The product conjugate was purified by membrane dialysis (MWCO 10 kDa) against PBS (2 × 2 L), and deionized water (3 × 2 L) over 2 days until impurities were lower than 5%, as determined by analytical UPLC. The dialyzed solution was collected and freeze-dried to afford **4** G5(LA)<sub>10</sub>(RF)<sub>5</sub> as a pale yellow solid. The number ( $n = 5 \pm 1$ ) of riboflavin molecules attached per dendrimer was estimated on a mean basis by UV-vis spectrometry. UPLC:  $t_r = 9.3$  min; purity >95%. MALDI TOF mass spectrometry ( $m/z$ , gmol<sup>-1</sup>): 41 000. <sup>1</sup>H NMR (500 MHz, D<sub>2</sub>O):  $\delta$  3.9 (br), 3.7–3.4 (m), 3.5–3.3 (br), 3.3–3.1 (br m), 2.95–2.75 (br), 2.75–2.6 (br m), 2.55–2.35 (br m), 2.3–2.15 (br m), 1.95 (m), 1.85 (m), 1.6 (br m), 1.4 (br) ppm. UV-vis (PBS, pH 7.4):  $\lambda_{\text{max}} = 448$  nm ( $\epsilon = 4045$  M<sup>-1</sup> cm<sup>-1</sup>; RF), 350 nm ( $\epsilon = 4847$  M<sup>-1</sup> cm<sup>-1</sup>; RF), 274 nm ( $\epsilon = 28\,800$  M<sup>-1</sup> cm<sup>-1</sup>).

**Preparation of AuNP.** Gold nanoparticles (AuNPs, mean diameter = 16 nm) were synthesized by an established method.<sup>56</sup> An aqueous solution of sodium citrate was added to a boiling solution of HAuCl<sub>4</sub> in water, each mixed at a ratio of [citrate]/[Au(III)] = 2.72 ([citrate] = 0.68 mM; [Au] = 0.25 mM). UV-vis (PBS, pH 7.4):  $\lambda_{\text{max}} = 520$  (522<sup>56</sup>) nm. Distribution of the size of AuNPs was measured by dynamic light scattering measured at 25 °C (z-average hydrodynamic diameter = 30.27 nm, PDI = 0.433; Figure S4, Supporting Information), and also by AFM (mean core diameter = 13.5 ± 2.2 nm vs 13 nm (TEM<sup>56</sup>)).

**Chemisorption of Lipoic Acid (LA)-Containing Dendrimers to AuNP (Figure 1A,B).** For dendrimer **3**–AuNP, **3** G5(LA)<sub>10</sub> (2.5 μM in water as a stock solution) was titrated into a solution of AuNP (2 mL; [Au] = 0.125 mM) in 10 μL increments. After each addition, the solution was mixed thoroughly, and its UV-vis spectrum was measured as summarized in Figure 1. Dendrimer **4**–AuNP was prepared in a similar manner.

**Complexation of Riboflavin Binding Protein (RfBP) with Dendrimer **4**–AuNP (Figure 1).** A solution of dendrimer **4**–AuNP was prepared as described above by reacting **4** (25 μM, 70 μL) with AuNP (2 mL). RfBP (3.3 μM) was titrated into this solution in 10 μL increments (each 0.5% increase in volume) until a saturation point was reached (~70 μL; ~3% increase relative to an initial volume). After each addition, the UV-vis spectrum was recorded as summarized in Figure 1.

**Substrate Preparation for AFM Imaging.** AuNP and its dendrimer nanoconjugates were imaged using a MultiMode Atomic Force Microscope (Bruker, Santa Barbara, CA). Bruker SCANASYST cantilevers of nominal 0.7 N/m spring constant and 120–180 kHz resonance frequency were used for AFM imaging in PBS buffer. Prior to imaging, the vertically engaging E-scanner was calibrated for accuracy in the x, y, z direction by using a 1 μm grid with a depth of 20 nm. Mica substrates were prepared for imaging as follows. Freshly cleaved mica was modified with a 100 μL deposit of 0.01% 3-(aminopropyl)-triethoxysilane (APTES) solution. After a 20 min incubation period, the mica surface was rinsed six times with 1 mL aliquots of nanopure water and dried with compressed nitrogen. The modified mica substrate was incubated for 5 min with 10 μL of conjugate AuNP and placed in the AFM fluid cell holder for imaging. All images were collected in fluid Scanasyst mode under PBS buffer (pH 7.4) with a scan rate of 1 Hz. Digital resolution of each image was 512 × 512 pixels.

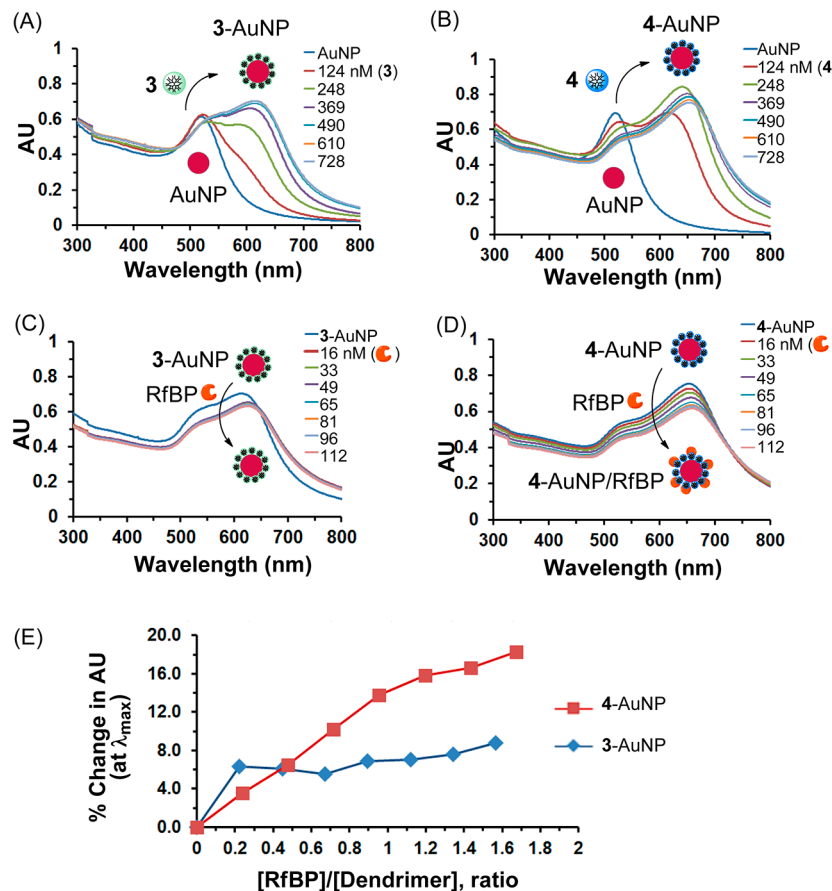


**Figure 1.** Proposed models for chemisorption of AuNPs by dendrimer nanoparticles 3 and 4 G5(LA)<sub>10</sub>(RF)<sub>n</sub> ( $n = 0, 5$ ). (A, B) Arrays of UV-vis spectra, each acquired during the titration of 3 G5(LA)<sub>10</sub> or 4 G5(LA)<sub>10</sub>(RF)<sub>5</sub> (2.5  $\mu$ M) into an AuNP solution in water ([AuNP] = 10 nM; 2 mL). Proposed models for interaction of RfBP with dendrimer chemisorbed AuNPs. Arrays of UV-vis spectra acquired during the titration of riboflavin binding protein (RfBP) to the surface-modified AuNPs (10 nM), each AuNP coated with 3 G5(LA)<sub>10</sub> (C) or 4 G5(LA)<sub>10</sub>(RF)<sub>5</sub> (D). The amount of dendrimer or RfBP indicated in the legend is expressed as a final concentration (nM) of the dendrimer or protein solution added. The plot in (E) summarizes the change (%) of absorption at the wavelength of  $\lambda_{\max}$  as a function of [RfBP]<sub>added</sub>/[Dendrimer].

**AFM Image Analysis.** All images were corrected for tip artifacts and surface bowing only, and analyzed using a Scanning Probe Image Processor (SPIP) software (version 6.0.2, Image Metrology A/S, Lyngby, Denmark). The particle size analysis was conducted by the Particle and Pore analysis module available in the SPIP software. An automatic threshold was applied for each image with particle sizes less than 7 nm excluded from the analysis. For the height analysis of AuNPs (a representative image shown in Figure 3A), seventeen 5  $\mu$ m  $\times$  5  $\mu$ m images were analyzed with  $\sim$ 700 NP per image ( $n = 12,063$ ). For the height analysis of dendrimer 4-AuNP (a representative image shown in Figure 3B), nine 10  $\mu$ m  $\times$  10  $\mu$ m images were analyzed with  $\sim$ 250 NP per image ( $n = 2281$ ). For the height analysis of dendrimer 4-AuNP + RfBP (a representative image shown in Figure 3C), nine 10  $\mu$ m  $\times$  10  $\mu$ m images were analyzed with  $\sim$ 280 NP per image ( $n = 2476$ ). For the height analysis of dendrimer 4-AuNP + RfBP + RF (a representative image shown in Figure 3D), twelve 10  $\mu$ m  $\times$  10  $\mu$ m images were analyzed with  $\sim$ 210 NP per image ( $n = 2551$ ). Histograms and kernel density function plots were generated to examine the height distribution of nanoparticles. All density curves reported were generated using 512 points and the Gaussian kernel function. Peak heights were obtained by fitting the density curve to the minimum number of Gaussians and

taking the peak value and the width of the Gaussian using the commercially available PeakFit software.

**Cell Culture.** KB cells were grown as a monolayer culture in a riboflavin-deficient RPMI 1640 medium supplemented with 10% fetal bovine serum (FBS), penicillin (100 IU/mL), and streptomycin (100  $\mu$ g/mL).<sup>23,33</sup> Cells were maintained at 37 °C under 5% CO<sub>2</sub>.

**Confocal Microscopy.** Fluorescence confocal imaging was performed following a standard method.<sup>23,33</sup> KB cells were seeded overnight on eight-well chambered cover glass slides at a density of 5  $\times$  10<sup>4</sup> cells/well (Lab-Tek). Cells were treated with 3-AuNP or 4-AuNP at different concentrations (50 or 80 nM) in media for 2 h or 4 h at 37 °C followed by washing with PBS (three times). The cells were fixed with 4% paraformaldehyde and mounted in ProLong Gold with 4,6-diamidino-2-phenylindole (DAPI) (Life Technologies). The signal from the SPR scattering of AuNPs was collected on a Leica inverted SPSX confocal microscope (Leica Microsystems) using a 63 $\times$  oil immersion objective. DAPI signal was used for locating cells for imaging. SPR of the AuNPs was measured by excitation with the white light laser at 514 nm, with sequential scanning of emission at 474–506 and 522–570 nm, similar to what was described previously.<sup>4</sup> Emissions from these two channels were overlaid to yield the total SPR scattering signal which was merged with a differential interference contrast (DIC) image.

## RESULTS AND DISCUSSION

**Synthesis and Characterization of Dendrimer Conjugates.** Conjugates 3 and 4 used in this study are based on a fifth generation (G5) poly(amido amine) (PAMAM) dendrimer G5-(NH<sub>2</sub>) (diameter 5.4 nm). We prepared each by conjugating G5-(NH<sub>2</sub>) with ( $\pm$ )- $\alpha$ -lipoic acid (LA) alone (3) or in combination with the RF ligand (4) as summarized in Scheme 1. In the design of these dendrimer conjugates, we introduced ( $\pm$ )- $\alpha$ -lipoic acid as a bifunctional molecule that provides both a carboxylic acid for dendrimer conjugation and a dithiolanyl moiety to serve as a disulfide handle for dendrimer chemisorption to the surface of AuNP through Au–S bond formation.

First, we prepared the 3 G5(LA)<sub>m=10</sub> conjugate (Scheme 1) by reaction of G5-(NH<sub>2</sub>)<sub>114</sub> with freshly prepared lipoic HOBT ester added at 15 molar equivalency to the dendrimer. After this amide coupling step, each of the unreacted surface amines was modified to N-glutaryl amide. The number (*m*) of lipoic acid molecules attached per dendrimer was estimated on a mean basis by the <sup>1</sup>H NMR integration method.<sup>33,51</sup> In this method, the integration area (AUC<sub>GA</sub>) for those CH<sub>2</sub> signals of the glutaric amide residue (each at  $\delta$  2.25, 2.20, 1.83 ppm; Figure S3, Supporting Information) was compared to the area (AUC<sub>LA</sub>) of those CH<sub>2</sub> signals of the lipoic amide residue (selected, each at 1.4, 1.6 ppm): *m* + *p* = 114, and *m/p* = AUC<sub>LA</sub>/AUC<sub>GA</sub> where *m* and *p* refer to the number of LA and GA residues, respectively.

Second, we prepared the conjugate 4 G5(LA)<sub>10</sub>(RF)<sub>5</sub> by amide conjugation of 3 G5(LA)<sub>10</sub> with a RF ligand 1 through an ethylenedioxybis(ethylamine) spacer. Here, 3-(carboxymethyl)riboflavin (1)<sup>54,57</sup> was selected as the RF ligand because of its carboxylic acid located at its N-3 position of an isoalloxazine head and the retained binding affinity of N-3 derivatives (e.g.,  $K_D$  = 2.5 nM for N-3 Me)<sup>58</sup> to riboflavin binding protein (RfBP). Thus each RF molecule was attached to the dendrimer through the two carbon spacers provided by 1 extended with the additional ethylene oxide-based spacer. This linker design aimed to provide a linker long enough for the dendrimer-attached RF to bind the targeted receptor protein without any steric constraint as supported by our prior studies based on cellular binding<sup>33</sup> and our SPR studies.<sup>31</sup> The synthetic method used for the conjugate 4 was based on a PyBop-based activation of 3 prior to the reaction with 2.

Each conjugate was purified by exhaustive dialysis using a membrane tubing (MWCO 10 kDa) until its purity was greater than 95% without detectable amounts of free LA and/or the RF ligand as determined by HPLC (Figure S1, Supporting Information). Each of these conjugates 3 and 4 was fully characterized by employing standard analytical techniques including UV-vis spectrometry, <sup>1</sup>H NMR spectroscopy, MALDI TOF mass spectrometry, and GPC (Table 1, Supporting Information). The UV-vis spectrum of 4 provides strong absorption at long wavelengths assigned for the isoalloxazine chromophore of RF (Figure S2, Supporting Information;  $\lambda_{\text{max}} = 449$  nm,<sup>32</sup>  $\epsilon = 12\,100\text{ M}^{-1}\text{ cm}^{-1}$ ). The analysis of such UV-vis spectral data allowed determination of the number (*n* = 5) of RF ligands attached to the dendrimer particle on a mean basis. Use of another complementary method based on <sup>1</sup>H NMR integration was inapplicable for this analysis due to the strong line broadening of RF aromatic proton signals. The efficiency for small molecule conjugation to the dendrimer ([ligand]<sub>attached</sub> vs [ligand]<sub>added</sub>) was approx-

**Table 1. Macromolecular Properties of G5 PAMAM Dendrimer Conjugates 3 and 4**

dendrimer conjugate	MW (g mol <sup>-1</sup> ) <sup>a</sup>	MW (g mol <sup>-1</sup> ) <sup>b</sup>	PDI <sup>c</sup>	R <sub>n</sub> (nm) <sup>d</sup>	purity (%) <sup>e</sup>
3 G5(LA) <sub>10</sub>	40 700	35 000	1.601	8.0	≥95
4 G5(LA) <sub>10</sub> (RF) <sub>5</sub>	41 000	43 000	2.164	15.5	≥95

<sup>a</sup>Measured by matrix assisted laser desorption ionization (MALDI) mass spectrometry. <sup>b</sup>Mean molecular weight ( $= [M_n + M_w] \div 2$ ) determined by gel permeation chromatography (GPC). <sup>c</sup>Polydispersity index (PDI) by GPC =  $M_w/M_n$ . <sup>d</sup>Hydrodynamic radius (RMS) calculated from  $M_n$ . <sup>e</sup>UPLC.

imately 70% for LA and 20% for the RF ligand. The conjugation efficiency is apparently lower for the second ligand with RF. This is possibly attributable to steric congestion by preexisting LA presented on the dendrimer surface,<sup>50</sup> as well as the in situ method used for linker extension.

**AuNP Functionalization through Chemisorption with Dendrimer Conjugates.** AuNPs were prepared as citrate-stabilized particles by the gold(III) reduction method performed at a ratio of ([citrate]/[Au(II)] = 2.72) as described elsewhere.<sup>56</sup> The surface plasmon resonance absorption spectrum of AuNPs was measured by UV-vis spectrometry (Figure 1). The maximal absorption band ( $\lambda_{\text{max}}$ ) at 520 nm and lack of longer  $\lambda_{\text{max}}$  absorption at 600–700 nm by gold ellipsoids and nanorods<sup>59</sup> (Figure 1) suggest that these AuNPs are spherical and in the nonaggregated state, in agreement with dynamic light scattering measurements which gave a hydrodynamic diameter of ~30 nm (z-average). This hydrodynamic size (the Stokes diameter calculated from the diffusion properties of tumbling, solvated particles) includes the contribution from the hydrated diffusion layer surrounding the AuNP core and is apparently much greater than the size determined by current AFM analysis (discussed below) showing that these AuNPs are spherical particles with a mean core diameter of  $13.5 \pm 2.2$  nm ( $1\sigma$  error) in buffered solution. This size analysis is in good agreement with the value published in the literature (13 nm)<sup>56</sup> determined by transmission electron microscopy (TEM).

Surface functionalization of AuNPs with dendrimer conjugates 3 and 4 was performed by Au–S chemisorption<sup>2,60–62</sup> through a mechanism that involves the reaction of the cyclic disulfide moiety at the terminus of the LA<sup>62</sup> with Au surface. Dendrimer chemisorption was performed by incubation of each conjugate solution with AuNPs in water, and its progress was monitored by UV-vis spectroscopy (Figure 1). Upon dendrimer incubation, a large red shift was observed in the UV-vis spectra for dendrimer 3–AuNP ( $\lambda_{\text{max}} = 615$  nm), and for dendrimer 4–AuNP ( $\lambda_{\text{max}} = 653$  nm). Such a red shift has previously been reported in the chemisorption of polymer molecules on gold surfaces<sup>62,63</sup> though the spectral shifts observed with our dendrimer nanoparticles were much greater. We believe that such shifts are not due to the formation of large dendrimer-mediated aggregates of AuNPs as supported by an AFM analysis to be presented later showing the size distribution of dendrimer 4–AuNP with a peak diameter of  $20.5 \pm 4.0$  nm. In each AuNP functionalization, the amount of the dendrimer particles required for maximal coverage of the AuNP surface was determined by the titration method as shown in Figure 1.

**UV–Vis Spectrometry for RfBP Complexation with Dendrimer-Coated AuNPs.** We investigated the interaction of RfBP with AuNPs modified with dendrimer 3 or 4 by UV–

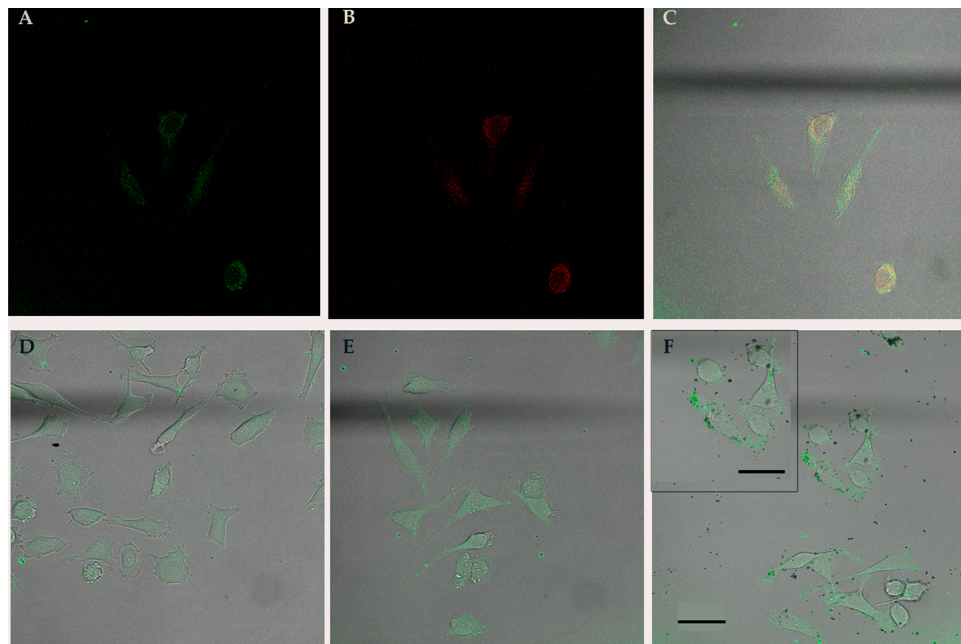


**Figure 2.** Cellular uptake of AuNP derived constructs in KB cells. (A)–(C) KB cells treated with 50 nM of unmodified AuNP for 2 h were imaged by (A) SPR scattering or (B) luminescence. (C) Co-localization of the signals was confirmed by the overlay. SPR scattering imaging was taken for KB cells treated for 4 h with 80 nM of (D) AuNP, (E) dendrimer 3–AuNP, or (F) dendrimer 4–AuNP (inset is a magnified view of the adjacent cells). Scale bar = 30.3  $\mu$ m (inset, 28.8  $\mu$ m). Confocal microscopic images (63 $\times$  magnification) were taken as described in the Experimental Section. Signal from the SPR scattering was overlaid with differential interference contrast (DIC) images. Data shown are representative of multiple images acquired for each treatment condition.

vis spectrometry (Figure 1). With incremental addition of RfBP to dendrimer 3–AuNP, the absorption bands decreased significantly at first but insignificantly later ( $\leq 5\%$ ) with a small shift in the wavelength of  $\lambda_{\text{max}}$  to 622 nm at saturation ( $\Delta$  wavelength = 7 nm; Figure 1D,E). Such spectral changes are quite distinct with those observed from dendrimer 4–AuNP, which showed a concentration-dependent decrease ( $\approx 16\%$ ) in absorption with a small red shift to 659 nm ( $\Delta$  wavelength = 6 nm; Figure 1D,E). This absorption decrease is significant and not due to increase ( $\approx 3\%$ ) in the volume of the solution that occurred during the titration. We attribute this spectral trend for dendrimer 4–AuNP to specific binding of RfBP to the RF ligand presented on the surface of AuNP-attached dendrimer. In contrast, there is no specific spectral trend indicative of specific binding of RfBP to dendrimer 3–AuNP that does not present RF ligands on the dendrimer surface though small extent of nonspecific binding or aggregation might occur with dendrimer 3–AuNP as suggested by the initial decrease and shift in the absorption. Thus UV-vis absorption spectral traces provide evidence for specific interaction of RfBP with RF-presenting dendrimer 4–AuNP.

**Confocal Microscopy of Dendrimer–AuNPs.** In addition to the UV titration study in solution, we performed a confocal imaging study *in vitro* for demonstrating the binding and uptake (collectively termed as “association”) of dendrimer 4–AuNP in KB cancer cells that express the RF receptors as described elsewhere.<sup>31–33</sup>

In terms of imaging modality, AuNPs display several optophysical properties such as surface plasmon resonance (SPR) absorption in the visible region of the light spectrum, visible luminescence, and SPR scattering effects. Due to these properties, AuNPs have recently attracted significant attention as visible probes for biological sensing and imaging studies for *in vitro* and *in vivo* applications.<sup>3–5,13</sup> In this study, we were

interested in their SPR scattering properties because detection of AuNPs in biological samples can occur without additional fluorescent labels or modifications. Following the imaging methods as demonstrated in previous studies using dark field light microscopy<sup>3,64,65</sup> and confocal microscopy,<sup>4</sup> we investigated whether AuNP or its dendrimer nanocomposites undergo cellular association in cancer cells *in vitro*.

We first verified the SPR scattering of AuNP as its detection modality using unmodified citrate-adsorbed AuNP (no fluorescent dye or chemisorbed dendrimer) in KB cancer cells. After a 2 h incubation with AuNP (50 nM), the treated KB cells were imaged by confocal microscopy with two different detection configurations: (i) scattered SPR (excitation 514 nm; emission 474–506 and 522–570 nm) and (ii) luminescence (excitation at 514 nm; emission at 550–650 nm) as shown in Figure 2A–C. AuNPs associated with the cells are clearly detectable both by SPR scattering and by luminescence, although their detection intensities are weak—indicative of the low level of cellular association. Thus, despite the lack of fluorescent dye molecules, it was possible to detect AuNPs associated with and internalized in the cells by two different imaging methods.

We next treated KB cells with AuNP, dendrimer 3–AuNP or dendrimer 4–AuNP, each at 80 nM, for 4 h, and imaged the treated cells in the SPR scattering mode as shown in Figure 2D–F. From these scattering images, qualitative differences between the AuNP and dendrimer–AuNP samples were observed. Cells treated with the riboflavin targeted dendrimer 4–AuNP showed more punctate and localized areas of signal which were distinctly more intense than those found in the bare AuNP and dendrimer 3–AuNP treated cells at this time point (Figure 2F). This scattering is attributable to aggregated AuNPs either on the cell surface or inside the cell. In summary, dendrimer chemisorbed 4–AuNPs were detectable by the SPR

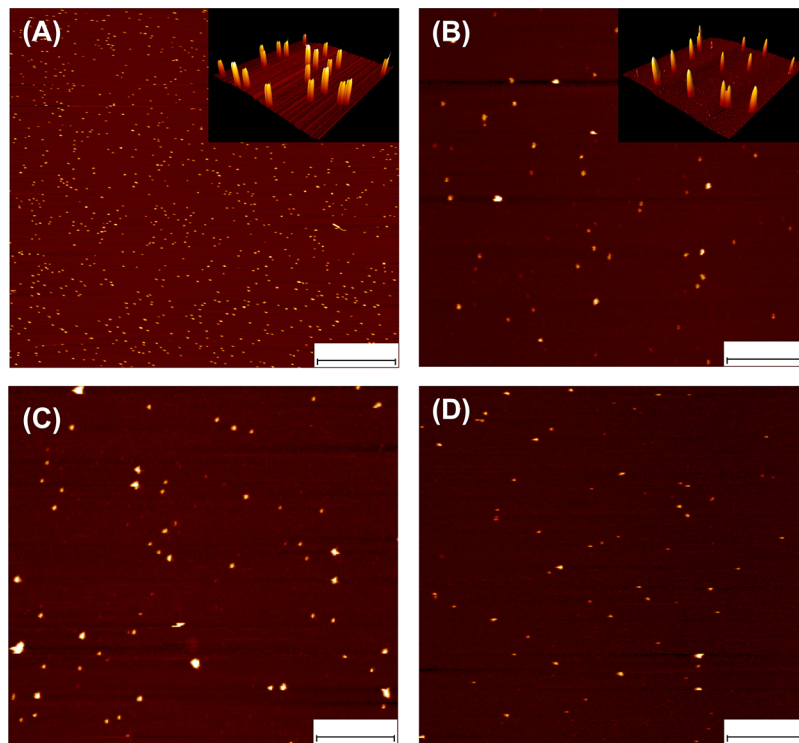


**Figure 3.** AFM images of AuNPs and dendrimer chemisorbed AuNPs on 0.01% APTES treated mica in PBS buffer (pH 7.4): (A) 2 nM AuNPs (*z*-scale 25 nm); (B) 7.5 ( $\pm$ 2.5) nM dendrimer 4–AuNP (*z*-scale 50 nm); (C) 7.5 ( $\pm$ 2.5) nM dendrimer 4–AuNP after the addition of 0.5  $\mu$ M RfBP (*z*-scale 60 nm); (D) 7.5 ( $\pm$ 2.5) nM dendrimer 4–AuNP with 0.5  $\mu$ M RfBP after the addition of 5  $\mu$ M RF (*z*-scale 30 nm). The scale bar is 1  $\mu$ m in size. Inset for (A) and (B): close-up view of the NPs imaged in air (1  $\mu$ m  $\times$  1  $\mu$ m).

scattering method using confocal microscopy, providing evidence for the cellular localization of these AuNPs. Our confocal microscopy studies demonstrated the utility of the dual detection modes of AuNPs based on SPR scattering and luminescence, both of which are inherent properties of AuNPs, for determining the cellular localization of AuNPs without the need for additional particle labeling.

**AFM Imaging of AuNPs on Mica Surface.** We employed mica as a substrate in AFM imaging due to its atomic flatness. However, the negative surface charge of mica makes immobilization of previously described nanoparticles unfavorable due to the presence of the negatively charged citrate groups on the surface of AuNPs (Figure S6A, Supporting Information). Similarly, the dendrimers conjugated to AuNPs have an overall negative charge due to excess linker branches containing glutaric acid ( $pK_a$  = 4.31, 5.41). To obtain an adequate surface coverage of conjugated and unconjugated gold nanoparticles, the mica surface needs to be pretreated to generate a positive surface charge. Common approaches used for functionalizing mica substrates are to treat the mica surface with  $MgCl_2$ ,<sup>66</sup>  $NiCl_2$ ,<sup>66</sup> or 3-(aminopropyl)triethoxysilane.<sup>67</sup> The  $MgCl_2$  treated mica surface did not, however, yield substantial coverage of AuNPs on the surface, resulting in only very few observable nanoparticles when imaged by AFM in PBS buffer (Figure S6B, Supporting Information). Similar observations have been noted with  $Mg^{2+}$  treated mica surfaces, and the immobilization appears to depend on the size of the nanoparticles with larger AuNPs not adhering to the  $MgCl_2$  treated mica surface.<sup>68</sup> 3-(Aminopropyl)triethoxysilane (APTES) treated mica is also commonly used for immobilizing biological material and has been used extensively in imaging DNA on mica substrates.<sup>67</sup> Mica substrates treated with 0.01%

APTES solution were found to be favorably disposed toward achieving electrostatic immobilization of unconjugated AuNPs (Figure 3A). The immobilization of conjugated AuNPs is also likely aided by the hydrophobic surface of the APTES–mica as opposed to the hydrophilic surface of a freshly cleaved mica surface.<sup>69</sup> The height of the unconjugated AuNPs from Figure 3A was found to be  $13.5 \pm 2.2$  nm (obtained from seventeen 5  $\mu$ m  $\times$  5  $\mu$ m images, each with  $\sim$ 700 NPs).

**AFM Imaging of Dendrimer Chemisorbed on AuNPs.** AFM was used to determine the height distribution of dendrimer 4–AuNPs for comparison with the height distribution of bare AuNPs ( $13.5 \pm 2.2$  nm) covered with citrate anions (Figure 3A,B). All AFM imaging work was carried out on 0.01% APTES modified mica substrates, as per the results of immobilization work presented above. Analysis of Figure 3A,B AFM images suggests an 83% decrease in surface density of the adsorbed 4–AuNPs (3B) in comparison to the bare AuNPs (3A). This is likely due to the overall charge on the bare AuNP being much more negative in comparison to the dendrimer 4–AuNP, resulting in less attraction of the conjugated AuNPs to the APTES modified mica surface. In addition, the conjugation of dendrimers to the AuNP via the longer lipoic amide-based linkers shields most of the negative charges otherwise conferred by citrate anions on the bare AuNP. It is also plausible that certain groups in the dendrimer 4 including the RF ligand attached ( $pK_a$  of pteridine head = 9.69<sup>70</sup>) and a minor fraction of internal tertiary amines (theoretically 126 per particle;  $pK_a$  = 6.3–6.85 for its conjugate acid<sup>71</sup>) might be protonated in PBS (pH 7.4). The presence of such positively charged groups could contribute to partial neutralization of the dendrimer surface or repulsive dendrimer

interaction with the APTES mica surface, leading to the decreased surface adsorption of 4–AuNP.

The height distribution of dendrimer 4–AuNPs shows predominantly two peaks, with the first larger peak at  $12.0 \pm 2.9$  nm and a second smaller peak at  $20.5 \pm 4.0$  nm, each from the simulated curve (Figure 4a). The shoulder observed at  $\sim 8$

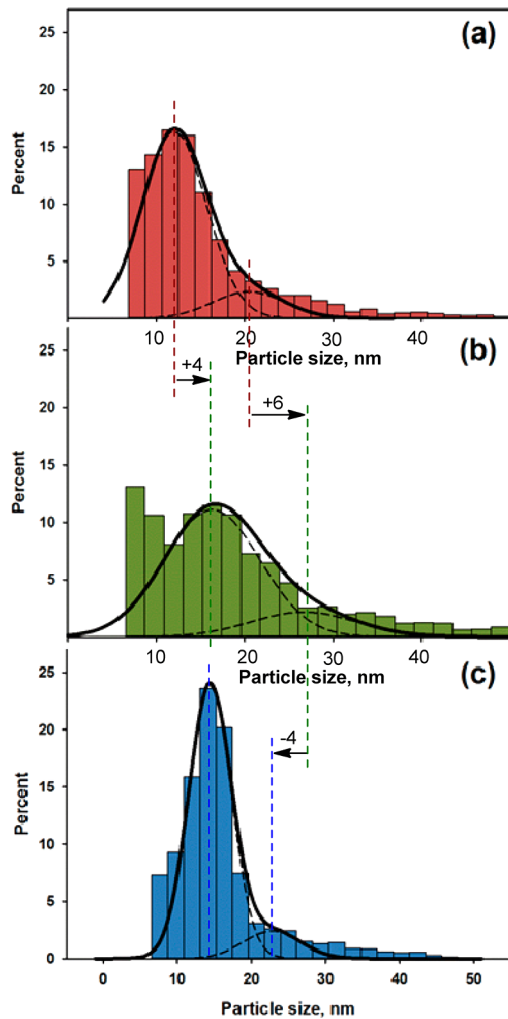


**Figure 4.** Nanoparticle height histogram plots: (a)  $7.5 (\pm 2.5)$  nM dendrimer 4–AuNP; (b)  $7.5 (\pm 2.5)$  nM dendrimer 4–AuNP after the addition of  $0.5 \mu\text{M}$  RfBP; (c)  $7.5 (\pm 2.5)$  nM dendrimer 4–AuNP with  $0.5 \mu\text{M}$  RfBP after the addition of  $5 \mu\text{M}$  RF. In each plot, dotted lines refer to simulated curves for the solid line.

nm is due to the 7 nm threshold applied in the data analysis and appears in all of the distributions presented in Figure 4; it will not be further discussed. The larger peak in height distribution (at  $20.5$  nm) is estimated in the range of  $+7$  nm of the peak height in the dendrimer 3–AuNP height distribution. This increase in size appears to be comparable to the size of individual dendrimer conjugates (mean diameter of a parent G5 dendrimer =  $5.4 \text{ nm}^{37}$ ) and suggests the formation of a dendrimer monolayer on the gold surface of the AuNP as proposed from the UV–vis titration experiments (Figure 1A,B). We believe that this heterogeneous distribution composed of the smaller and larger particles of dendrimer 4–AuNP might be attributable to the distribution in the number of dendrimer particles adsorbed on each AuNP with the larger size corresponding to AuNPs with higher numbers of adsorbed

dendrimers. It is notable that this distribution was detectable by AFM, but not by standard UV–vis spectrometric titration (Figure 1).

**AFM Imaging for Protein Interaction with Dendrimer on AuNPs.** We next investigated the interaction of RfBP with dendrimer 4 adsorbed on AuNP by AFM. First, the dendrimer 4–AuNP was imaged in the presence of  $0.5 \mu\text{M}$  RfBP (Figure 3C), and then binding of the RfBP to dendrimer surface was selectively blocked by addition of  $5.0 \mu\text{M}$  RF as a competitive ligand (Figure 3D). The height distributions of dendrimer 4–AuNPs under each of these conditions are represented as histograms in Figure 4b,c and as kernel density function plots in Figure 5.

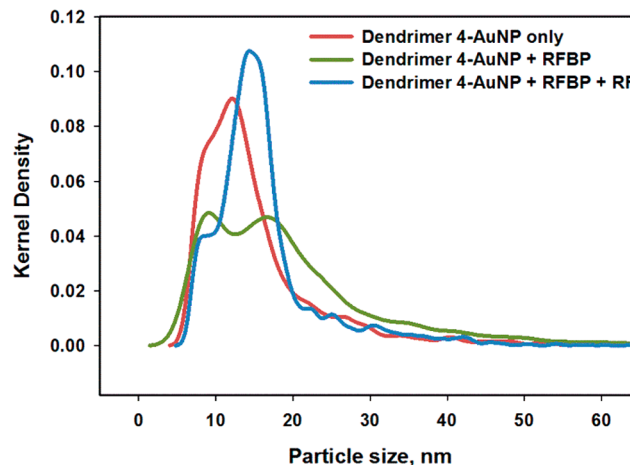


**Figure 5.** Kernel density plot showing height distribution analysis of each step of a three-step competitive binding experiment. Step 1:  $7.5 (\pm 2.5)$  nM dendrimer 4–AuNP imaged on modified mica under PBS buffer (red line). Step 2:  $0.5 \mu\text{M}$  RF-targeting RfBP was added to dendrimer 4–AuNP (green line). Step 3:  $5.0 \mu\text{M}$  RF was added to dendrimer 4–AuNP with  $0.5 \mu\text{M}$  RfBP (blue line).

Binding of RfBP to the dendrimer 4–AuNPs is indicated by peak height shifts to  $16.3 \pm 5.0$  nm with a broad shoulder centered at  $26.7 \pm 4.5$  nm (Figure 4B). These shifts correspond to approximately 4 and 6 nm increases in each of the peak heights, respectively, relative to untreated dendrimer 4–AuNP alone. We hypothesize that these observed height increases upon RfBP addition could reflect the number of RfBP molecules bound, and the heterogeneity in the RF ligand density on the dendrimer 4–AuNP. Recently, a number of reports have shown evidence that ligand conjugation to dendrimers through conventional methods such as amide coupling is unable to produce dendrimers with precisely defined ligand valency but rather yields stochastic distributions of ligand valencies.<sup>72–75</sup> In this study, we assigned a valency of five RF ligands attached per dendrimer for dendrimer 4. However, this ligand valency is calculated on an average basis, as dendrimer 4 is composed of mixed ligand valencies with a theoretical Poisson distribution (Figure S5, Supporting Information). Therefore, we believe that fewer RfBP molecules bind to those dendrimer 4–AuNPs coated with lower-valent dendrimer species compared to those with higher-valent species.

Second, we analyzed the number density of nanoparticles in the broad  $20\text{--}40$  nm range, which was significantly greater than the particle height at the main peak. This density comparison suggests that RfBP binding to the dendrimer 4–AuNPs

resulted in an increase in this population (from 17.0% to 28.9%; Table S1, Supporting Information). A binomial proportions test showed this increase to be significant ( $p < 0.05$ ) (Figure S7, Supporting Information). To confirm that this increase was due to the binding of RfBP to dendrimer 4, free RF (5  $\mu\text{M}$ ) was added to competitively bind RfBP in the medium and thereby prevent RfBP from binding to dendrimer 4–AuNP. The resulting peak height distributions show peaks centered at  $14.4 \pm 2.7$  and  $22.8 \pm 3.9$  nm (Figure 4C). In addition, a comparison of the height distribution of the nanoparticles after the addition of RF shows the density of nanoparticles in the 20–40 nm range decreased from 28.9% to 17.4%, a statistically significant change ( $p < 0.05$ ; Figure S7, Supporting Information). The kernel density (Figure 5) in the 20–40 nm region for dendrimer 4–AuNP, prior to the addition of RfBP and after the competitive binding of RF with RfBP, shows a modest change in particle density from 17.0% to 17.4%, which, on the basis of the binomial proportions test, shows no statistical significance ( $p = 0.45$ ).

## CONCLUSIONS

We designed and characterized a dendrimer–AuNP nanocomposite as a potential RF receptor targeted delivery system. We probed its receptor binding *in vitro* by using an array of complementary methods including UV–vis spectroscopy, confocal SPR imaging and AFM. First, we illustrated the capability of AFM as a quantitative method for investigating receptor–ligand interactions at the AuNP–dendrimer interface. In this AFM approach, specific binding of RfBP to RF-presenting dendrimer–AuNP was probed by detecting changes in particle height distribution as a metric. Such AFM-based quantitative analysis is not achievable by corresponding UV–vis spectrometric titration experiments or confocal image analysis. Second, our AFM study suggests preexisting heterogeneity in the RF ligand distribution on dendrimers as the basis that leads to heterogeneous populations of RfBP bound to the dendrimer-adsorbed AuNP. These results corroborate a model for the RF receptor–ligand interaction suggested by UV–vis spectrometry and confocal microscopic studies. This study clearly demonstrates that AFM serves as an imaging tool for the determination of size distributions as well as for quantifying receptor–ligand interaction at the AuNP–protein interface under a nearly physiological condition.

## ASSOCIATED CONTENT

### Supporting Information

HPLC and GPC traces, UV–vis and  $^1\text{H}$  NMR spectra, Z-average size distribution, Poissonian distribution, AFM images, binomial proportion analysis, and binomial plot. This material is available free of charge via the Internet at <http://pubs.acs.org>.

## AUTHOR INFORMATION

### Corresponding Authors

\*K. Sinniah: phone, (616) 526-6058; fax, (616) 526-6501; e-mail, [ksinniah@calvin.edu](mailto:ksinniah@calvin.edu).

\*S. K. Choi: phone, (734) 615-0618; fax, (734) 615-0621, e-mail, [skchoi@umich.edu](mailto:skchoi@umich.edu).

### Author Contributions

||A. B. Witte and A. N. Leistra contributed equally to this work.

### Notes

The authors declare no competing financial interest.

## ACKNOWLEDGMENTS

Part of this work was supported by NCI, NIH under award 1 R01 CA119409, and University of Michigan Office of the Vice President for Research and Shanghai Jiao Tong University (SKC). SKC thanks support from Undergraduate Research Opportunity Program at University of Michigan. KS acknowledges the support of NSF (CHE-0959681) and HHMI (student support) at Calvin College.

## REFERENCES

- (1) Giljohann, D. A.; Seferos, D. S.; Daniel, W. L.; Massich, M. D.; Patel, P. C.; Mirkin, C. A. Gold Nanoparticles for Biology and Medicine. *Angew. Chem., Int. Ed.* **2010**, *49*, 3280–3294.
- (2) Daniel, M.-C.; Astruc, D. Gold Nanoparticles; Assembly, Supramolecular Chemistry, Quantum-Size-Related Properties, and Applications toward Biology, Catalysis, and Nanotechnology. *Chem. Rev. (Washington, DC, U. S.)* **2004**, *104*, 293–346.
- (3) El-Sayed, I. H.; Huang, X.; El-Sayed, M. A. Surface Plasmon Resonance Scattering and Absorption of anti-EGFR Antibody Conjugated Gold Nanoparticles in Cancer Diagnostics: Applications in Oral Cancer. *Nano Lett.* **2005**, *5*, 829–834.
- (4) Klein, S.; Petersen, S.; Taylor, U.; Barcikowski, S.; Rath, D. Quantitative visualization of colloidal and intracellular gold nanoparticles by confocal microscopy. *J. Biomed. Opt.* **2010**, *15*, 036015–036015.
- (5) Raschke, G.; Kowarik, S.; Franzl, T.; Sönnichsen, C.; Klar, T. A.; Feldmann, J.; Nichtl, A.; Kürzinger, K. Biomolecular Recognition Based on Single Gold Nanoparticle Light Scattering. *Nano Lett.* **2003**, *3*, 935–938.
- (6) Huang, W.-C.; Tsai, P.-J.; Chen, Y.-C. Functional gold nanoparticles as photothermal agents for selective-killing of pathogenic bacteria. *Nanomedicine* **2007**, *2*, 777–787.
- (7) Lim, Y. T.; Cho, M. Y.; Choi, B. S.; Noh, Y.-W.; Chung, B. H. Diagnosis and therapy of macrophage cells using dextran-coated near-infrared responsive hollow-type gold nanoparticles. *Nanotechnology* **2008**, *19*, 375105.
- (8) Visaria, R. K.; Griffin, R. J.; Williams, B. W.; Ebbini, E. S.; Paciotti, G. F.; Song, C. W.; Bischof, J. C. Enhancement of tumor thermal therapy using gold nanoparticle-assisted tumor necrosis factor- $\alpha$  delivery. *Mol. Cancer Ther.* **2006**, *5*, 1014–1020.
- (9) Choi, W. I.; Kim, J.-Y.; Kang, C.; Byeon, C. C.; Kim, Y. H.; Tae, G. Tumor Regression *In Vivo* by Photothermal Therapy Based on Gold-Nanorod-Loaded, Functional Nanocarriers. *ACS Nano* **2011**, *5*, 1995–2003.
- (10) Lin, C.-C.; Yeh, Y.-C.; Yang, C.-Y.; Chen, G.-F.; Chen, Y.-C.; Wu, Y.-C.; Chen, C.-C. Quantitative analysis of multivalent interactions of carbohydrate-encapsulated gold nanoparticles with concanavalin A. *Chem. Commun. (Cambridge, U. K.)* **2003**, 2920–2921.
- (11) Gültekin, A.; Ersöz, A.; Hür, D.; Sarlözü, N. Y.; Denizli, A.; Say, R. Gold nanoparticles having dipicolinic acid imprinted nanoshell for *Bacillus cereus* spores recognition. *Appl. Surf. Sci.* **2009**, *256*, 142–148.
- (12) Xiao, Q.; Gao, H.; Lu, C.; Yuan, Q. Gold nanoparticle-based optical probes for sensing aminothiols. *TrAC, Trends Anal. Chem.* **2012**, *40*, 64–76.
- (13) Liu, H.; Xu, Y.; Wen, S.; Chen, Q.; Zheng, L.; Shen, M.; Zhao, J.; Zhang, G.; Shi, X. Targeted Tumor Computed Tomography Imaging Using Low-Generation Dendrimer-Stabilized Gold Nanoparticles. *Chem. - Eur. J.* **2013**, *19*, 6409–6416.
- (14) Patra, C. R.; Bhattacharya, R.; Mukhopadhyay, D.; Mukherjee, P. Fabrication of gold nanoparticles for targeted therapy in pancreatic cancer. *Adv. Drug Delivery Rev.* **2010**, *62*, 346–361.
- (15) Heo, D. N.; Yang, D. H.; Moon, H.-J.; Lee, J. B.; Bae, M. S.; Lee, S. C.; Lee, W. J.; Sun, I.-C.; Kwon, I. K. Gold nanoparticles surface-functionalized with paclitaxel drug and biotin receptor as theranostic agents for cancer therapy. *Biomaterials* **2012**, *33*, 856–866.
- (16) Abdelhady, H. G.; Allen, S.; Davies, M. C.; Roberts, C. J.; Tendler, S. J. B.; Williams, P. M. Atomic force microscopy studies of

- generation 4 poly(amidoamine) (PAMAM) dendrimers on functionalized surfaces. *Surf. Sci.* **2004**, *558*, 99–110.
- (17) Liu, H.; Shen, M.; Zhao, J.; Zhu, J.; Xiao, T.; Cao, X.; Zhang, G.; Shi, X. Facile formation of folic acid-modified dendrimer-stabilized gold-silver alloy nanoparticles for potential cellular computed tomography imaging applications. *Analyst* **2013**, *138*, 1979–1987.
- (18) White, H. B.; Merrill, A. H. Riboflavin-Binding Proteins. *Annu. Rev. Nutri.* **1988**, *8*, 279–299.
- (19) Karande, A. A.; Sridhar, L.; Gopinath, K. S.; Adiga, P. R. Riboflavin carrier protein: a serum and tissue marker for breast carcinoma. *Int. J. Cancer* **2001**, *95*, 277–281.
- (20) Johnson, T.; Ouhtit, A.; Gaur, R.; Fernando, A.; Schwarzenberger, P.; Su, J.; Ismail, M. F.; El-Sayyad, H. I.; Karande, A.; Elmagreed, Z. A.; Rao, P.; Raj, M. Biochemical characterization of riboflavin carrier protein (RCP) in prostate cancer. *Front. Biosci., Landmark Ed.* **2009**, *14*, 3634–3640.
- (21) Hilgenbrink, A. R.; Low, P. S. Folate receptor-mediated drug targeting: From therapeutics to diagnostics. *J. Pharm. Sci.* **2005**, *94*, 2135–2146.
- (22) Lee, R. J.; Low, P. S. Folate-mediated tumor cell targeting of liposome-entrapped doxorubicin in vitro. *Biochim. Biophys. Acta, Biomembr.* **1995**, *1233*, 134–144.
- (23) Silpe, J. E.; Sumit, M.; Thomas, T. P.; Huang, B.; Kotlyar, A.; van Dongen, M. A.; Banaszak Holl, M. M.; Orr, B. G.; Choi, S. K. Avidity Modulation of Folate-Targeted Multivalent Dendrimers for Evaluating Biophysical Models of Cancer Targeting Nanoparticles. *ACS Chem. Biol.* **2013**, *8*, 2063–2071.
- (24) Montet, X.; Funovics, M.; Montet-Abou, K.; Weissleder, R.; Josephson, L. Multivalent Effects of RGD Peptides Obtained by Nanoparticle Display. *J. Med. Chem.* **2006**, *49*, 6087–6093.
- (25) Shukla, R.; Thomas, T. P.; Peters, J.; Kotlyar, A.; Myc, A.; Baker, J. R., Jr. Tumor angiogenic vasculature targeting with PAMAM dendrimer-RGD conjugates. *Chem. Commun. (Cambridge, U. K.)* **2005**, 5739–5741.
- (26) Temming, K.; Lacombe, M.; Schaapveld, R. Q. J.; Orfi, L.; Kéri, G.; Poelstra, K.; Molema, G.; Kok, R. J. Rational Design of RGD–Albumin Conjugates for Targeted Delivery of the VEGF-R Kinase Inhibitor PTK787 to Angiogenic Endothelium. *ChemMedChem* **2006**, *1*, 1200–1203.
- (27) Chen, Y.; Foss, C. A.; Byun, Y.; Nimmagadda, S.; Pullambhatla, M.; Fox, J. J.; Castanares, M.; Lupold, S. E.; Babich, J. W.; Mease, R. C.; Pomper, M. G. Radiohalogenated Prostate-Specific Membrane Antigen (PSMA)-Based Ureas as Imaging Agents for Prostate Cancer. *J. Med. Chem.* **2008**, *51*, 7933–7943.
- (28) Shukla, R.; Thomas, T. P.; Desai, A. M.; Kotlyar, A.; Park, S. J.; Baker, J. R., Jr. HER2 specific delivery of methotrexate by dendrimer conjugated anti-HER2 mAb. *Nanotechnology* **2008**, *19*, 295102.
- (29) Thomas, T. P.; Shukla, R.; Kotlyar, A.; Liang, B.; Ye, J. Y.; Norris, T. B.; Baker, J. R., Jr. Dendrimer-Epidermal Growth Factor Conjugate Displays Superagonist Activity. *Biomacromolecules* **2008**, *9*, 603–609.
- (30) Raha, S.; Paunesku, T.; Woloschak, G. Peptide-mediated cancer targeting of nanoconjugates. *Wiley Interdiscip. Rev.: Nanomed. Nanobiotechnol.* **2010**, *3*, 269–281.
- (31) Plantinga, A.; Witte, A.; Li, M.-H.; Harmon, A.; Choi, S. K.; Banaszak Holl, M. M.; Orr, B. G.; Baker, J. R., Jr.; Sinniah, K. Bioanalytical Screening of Riboflavin Antagonists for Targeted Drug Delivery—A Thermodynamic and Kinetic Study. *ACS Med. Chem. Lett.* **2011**, *2*, 363–367.
- (32) Witte, A. B.; Timmer, C. M.; Gam, J. J.; Choi, S. K.; Banaszak Holl, M. M.; Orr, B. G.; Baker, J. R.; Sinniah, K. Biophysical Characterization of a Riboflavin-conjugated Dendrimer Platform for Targeted Drug Delivery. *Biomacromolecules* **2012**, *13*, 507–516.
- (33) Thomas, T. P.; Choi, S. K.; Li, M.-H.; Kotlyar, A.; Baker, J. R., Jr. Design of Riboflavin-Presenting PAMAM Dendrimers as a New Nanoplatform for Cancer-Targeted Delivery. *Bioorg. Med. Chem. Lett.* **2010**, *20*, 5191–5194.
- (34) Choi, Y.; Mecke, A.; Orr, B. G.; Banaszak Holl, M. M.; Baker, J. R. DNA-Directed Synthesis of Generation 7 and 5 PAMAM Dendrimer Nanoclusters. *Nano Lett.* **2004**, *4*, 391–397.
- (35) Li, J.; Piehler, L. T.; Qin, D.; Baker, J. R.; Tomalia, D. A.; Meier, D. J. Visualization and Characterization of Poly(amidoamine) Dendrimers by Atomic Force Microscopy. *Langmuir* **2000**, *16*, 5613–5616.
- (36) Mecke, A.; Majoros, I. J.; Patri, A. K.; Baker, J. R.; Banaszak Holl, M. M.; Orr, B. G. Lipid Bilayer Disruption by Polycationic Polymers: The Roles of Size and Chemical Functional Group. *Langmuir* **2005**, *21*, 10348–10354.
- (37) Tomalia, D. A.; Naylor, A. M.; William A. Goddard, I. Starburst Dendrimers: Molecular-Level Control of Size, Shape, Surface Chemistry, Topology, and Flexibility from Atoms to Macroscopic Matter. *Angew. Chem., Int. Ed.* **1990**, *29*, 138–175.
- (38) Zhang, Z.-L.; Pang, D.-W.; Yuan, H.; Cai, R.-X.; Abruña, H. Electrochemical DNA sensing based on gold nanoparticle amplification. *Anal. Bioanal. Chem.* **2005**, *381*, 833–838.
- (39) Prado-Gotor, R.; Grueso, E. A kinetic study of the interaction of DNA with gold nanoparticles: mechanistic aspects of the interaction. *Phys. Chem. Chem. Phys.* **2011**, *13*, 1479–1489.
- (40) Li, H.; Li, Z.; Wu, L.; Zhang, Y.; Yu, M.; Wei, L. Constructing Metal Nanoparticle Multilayers with Polyphenylene Dendrimer/Gold Nanoparticles via “Click” Chemistry. *Langmuir* **2013**, *29*, 3943–3949.
- (41) Huang, K.; Anne, A.; Bahri, M. A.; Demaille, C. Probing Individual Redox PEGylated Gold Nanoparticles by Electrochemical–Atomic Force Microscopy. *ACS Nano* **2013**, *7*, 4151–4163.
- (42) Li, D.; He, Q.; Cui, Y.; Li, J. Fabrication of pH-Responsive Nanocomposites of Gold Nanoparticles/Poly(4-vinylpyridine). *Chem. Mater.* **2007**, *19*, 412–417.
- (43) Crespo-Biel, O.; Dordi, B.; Reinoudt, D. N.; Huskens, J. Supramolecular Layer-by-Layer Assembly: Alternating Adsorptions of Guest- and Host-Functionalized Molecules and Particles Using Multivalent Supramolecular Interactions. *J. Am. Chem. Soc.* **2005**, *127*, 7594–7600.
- (44) Hansma, H. G.; Kasuya, K.; Oroudjev, E. Atomic force microscopy imaging and pulling of nucleic acids. *Curr. Opin. Struct. Biol.* **2004**, *14*, 380–385.
- (45) Hinterdorfer, P.; Baumgartner, W.; Gruber, H. J.; Schilcher, K.; Schindler, H. Detection and localization of individual antibody-antigen recognition events by atomic force microscopy. *Proc. Natl. Acad. Sci. U. S. A.* **1996**, *93*, 3477–3481.
- (46) Legleiter, J.; Kowalewski, T. Tapping, pulling, probing: atomic force microscopy in drug discovery. *Drug Discovery Today: Technol.* **2004**, *1*, 163–169.
- (47) Edwardson, J. M.; Henderson, R. M. Atomic force microscopy and drug discovery. *Drug Discovery Today* **2004**, *9*, 64–71.
- (48) Nakanishi, M.; Noguchi, A. Confocal and probe microscopy to study gene transfection mediated by cationic liposomes with a cationic cholesterol derivative. *Adv. Drug Delivery Rev.* **2001**, *52*, 197–207.
- (49) Schranz, M.; Baumann, R.-P.; Rhinow, D.; Hampp, N. Dynamics of Bacteriorhodopsin in Solid-Supported Purple Membranes Studied with Tapping-Mode Atomic Force Microscopy. *J. Phys. Chem. B* **2010**, *114*, 9047–9053.
- (50) Choi, S. K.; Leroueil, P.; Li, M.-H.; Desai, A.; Zong, H.; Van Der Spek, A. F. L.; Baker, J. R., Jr. Specificity and Negative Cooperativity in Dendrimer–Oxime Drug Complexation. *Macromolecules* **2011**, *44*, 4026–4029.
- (51) Choi, S. K.; Thomas, T.; Li, M.; Kotlyar, A.; Desai, A.; Baker, J. R., Jr. Light-Controlled Release of Caged Doxorubicin from Folate Receptor-Targeting PAMAM Dendrimer Nanoconjugate. *Chem. Commun. (Cambridge, U. K.)* **2010**, *46*, 2632–2634.
- (52) Majoros, I. J.; Thomas, T. P.; Mehta, C. B.; Baker, J. R., Jr. Poly(amidoamine) Dendrimer-Based Multifunctional Engineered Nanodevice for Cancer Therapy. *J. Med. Chem.* **2005**, *48*, 5892–5899.
- (53) Choi, S. K.; Thomas, T. P.; Leroueil, P. R.; Kotlyar, A.; Van Der Spek, A. F. L.; Baker, J. R. Specific and Cooperative Interactions between Oximes and PAMAM Dendrimers as Demonstrated by <sup>1</sup>H NMR Study. *J. Phys. Chem. B* **2012**, *116*, 10387–10397.

- (54) Caelen, I.; Kalman, A.; Wahlstrom, L. Biosensor-Based Determination of Riboflavin in Milk Samples. *Anal. Chem.* **2003**, *76*, 137–143.
- (55) Wu, F. Y. H.; MacKenzie, R. E.; McCormick, D. B. Kinetics and mechanism of oxidation-reduction reactions between pyridine nucleotides and flavins. *Biochemistry* **1970**, *9*, 2219–2224.
- (56) Ghosh, S. K.; Pal, A.; Kundu, S.; Nath, S.; Pal, T. Fluorescence quenching of 1-methylaminopyrene near gold nanoparticles: size regime dependence of the small metallic particles. *Chem. Phys. Lett.* **2004**, *395*, 366–372.
- (57) Merrill, A. H.; McCormick, D. B. Flavin affinity chromatography: General methods for purification of proteins that bind riboflavin. *Anal. Biochem.* **1978**, *89*, 87–102.
- (58) Nishina, Y.; Horiike, K.; Shiga, K.; Yamano, T. A fluorescence study of egg white riboflavin-binding protein. *J. Biochem.* **1977**, *82*, 1715–1721.
- (59) Liz-Marzán, L. M. Tailoring Surface Plasmons through the Morphology and Assembly of Metal Nanoparticles. *Langmuir* **2005**, *22*, 32–41.
- (60) Love, J. C.; Estroff, L. A.; Kriebel, J. K.; Nuzzo, R. G.; Whitesides, G. M. Self-Assembled Monolayers of Thiolates on Metals as a Form of Nanotechnology. *Chem. Rev. (Washington, DC, U. S.)* **2005**, *105*, 1103–1170.
- (61) Shan, J.; Tenhu, H. Recent advances in polymer protected gold nanoparticles: synthesis, properties and applications. *Chem. Commun. (Cambridge, U. K.)* **2007**, *0*, 4580–4598.
- (62) Mangeney, C.; Ferrage, F.; Aujard, I.; Marchi-Artzner, V.; Jullien, L.; Ouari, O.; Rékai, E. D.; Laschewsky, A.; Vikholm, I.; Sadowski, J. W. Synthesis and Properties of Water-Soluble Gold Colloids Covalently Derivatized with Neutral Polymer Monolayers. *J. Am. Chem. Soc.* **2002**, *124*, 5811–5821.
- (63) Salmaso, S.; Caliceti, P.; Amendola, V.; Meneghetti, M.; Magnusson, J. P.; Pasparakis, G.; Alexander, C. Cell up-take control of gold nanoparticles functionalized with a thermoresponsive polymer. *J. Mater. Chem.* **2009**, *19*, 1608–1615.
- (64) El-Sayed, I. H.; Huang, X.; El-Sayed, M. A. Selective laser photothermal therapy of epithelial carcinoma using anti-EGFR antibody conjugated gold nanoparticles. *Cancer Lett. (N. Y., NY, U. S.)* **2006**, *239*, 129–135.
- (65) Qian, W.; Huang, X.; Kang, B.; El-Sayed, M. A. Dark-field light scattering imaging of living cancer cell component from birth through division using bioconjugated gold nanoprobes. *J. Biomed. Opt.* **2010**, *15*, 046025–046029.
- (66) Abdelhady, H.; Allen, S.; Ebbens, S.; Madden, C.; Patel, N.; Roberts, C.; Zhang, J. Towards nanoscale metrology for biomolecular imaging by atomic force microscopy. *Nanotechnol.* **2005**, *16*, 966–973.
- (67) Umemura, K.; Ishikawa, M.; Kuroda, R. Controlled Immobilization of DNA Molecules Using Chemical Modification of Mica Surfaces for Atomic Force Microscopy: Characterization in Air. *Anal. Biochem.* **2001**, *290*, 232–237.
- (68) Vinelli, A.; Primiceri, E.; Brucale, M.; Zuccheri, G.; Rinaldi, R.; Samorì, B. Sample preparation for the quick sizing of metal nanoparticles by atomic force microscopy. *Microsc. Res. Tech.* **2008**, *71*, 870–879.
- (69) Bezanilla, M.; Manne, S.; Laney, D. E.; Lyubchenko, Y. L.; Hansma, H. G. Adsorption of DNA to Mica, Silylated Mica, and Minerals: Characterization by Atomic Force Microscopy. *Langmuir* **1995**, *11*, 655–659.
- (70) CRC Handbook of Chemistry and Physics: A Ready-reference Book of Chemical and Physical Data, 84th Ed ed.; Lide, D. R., Ed.; CRC Press: Boca Raton, FL, 1993.
- (71) Diallo, M. S.; Christie, S.; Swaminathan, P.; Balogh, L.; Shi, X.; Um, W.; Papelis, C.; Goddard, W. A.; Johnson, J. H. Dendritic Chelating Agents. 1. Cu(II) Binding to Ethylene Diamine Core Poly(amidoamine) Dendrimers in Aqueous Solutions. *Langmuir* **2004**, *20*, 2640–2651.
- (72) Mullen, D.; Borgmeier, E.; Desai, A.; van Dongen, M.; Barash, M.; Cheng, X. m.; Baker, J. R., Jr.; Banaszak Holl, M. Isolation and Characterization of Dendrimer with Precise Numbers of Functional Groups. *Chem. - Eur. J.* **2010**, *16*, 10675–10678.
- (73) Mullen, D. G.; Banaszak Holl, M. M. Heterogeneous Ligand–Nanoparticle Distributions: A Major Obstacle to Scientific Understanding and Commercial Translation. *Acc. Chem. Res.* **2011**, *44*, 1135–1145.
- (74) Mullen, D. G.; Desai, A. M.; Waddell, J. N.; Cheng, X.-m.; Kelly, C. V.; McNerny, D. Q.; Majoros, I. n. J.; Baker, J. R., Jr.; Sander, L. M.; Orr, B. G.; Banaszak Holl, M. M. The Implications of Stochastic Synthesis for the Conjugation of Functional Groups to Nanoparticles. *Bioconjugate Chem.* **2008**, *19*, 1748–1752.
- (75) Choi, S. K.; Myc, A.; Silpe, J. E.; Sumit, M.; Wong, P. T.; McCarthy, K.; Desai, A. M.; Thomas, T. P.; Kotlyar, A.; Holl, M. M. B.; Orr, B. G.; Baker, J. R. Dendrimer-Based Multivalent Vancomycin Nanoplatform for Targeting the Drug-Resistant Bacterial Surface. *ACS Nano* **2013**, *7*, 214–228.